ACS APPLIED MATERIALS & INTERFACES

Research Article

www.acsami.org

Facile Fabrication and Enhanced Sensing Properties of Hierarchically Porous CuO Architectures

Guoxing Zhu,[†] Huan Xu,[†] Yunyun Xiao,[†] Yuanjun Liu,[‡] Aihua Yuan,[‡] and Xiaoping Shen*[,†]

[†]School of Chemistry and Chemical Engineering, Jiangsu University, and [‡]School of Biology and Chemical Engineering, Jiangsu University of Science and Technology, Zhenjiang, 212013, China

Supporting Information

ABSTRACT: Hierarchically porous CuO architectures were successfully fabricated via copper basic carbonate precursor obtained with a facile hydrothermal route. The shape of the precursor is preserved after its conversion to porous CuO architectures by calcination. The obtained CuO are systemically characterized by X-ray powder diffraction, scanning electron microscopy, transmission electron microscopy, and Brunauer–Emmett–Teller N_2 adsorption–desorption analysis. The results reveal that hierarchical CuO microspheres are monoclinic structure and are assembled by porous single-crystal submicroplatelets. The Brunauer–Emmett–Teller N_2 adsorption–desorption analysis indicates that the obtained CuO has a surface area of 12.0 m^2/g with pore size of around 30 nm. The gas sensing performance of the as-prepared hierarchical CuO microspheres were investigated towards a series of typical organic solvents and fuels. They exhibit higher sensing response than that of commercial CuO powder. Their sensing properties can be further improved by loading of Ag nanoparticles on them, suggesting their potential applications in gas sensors.

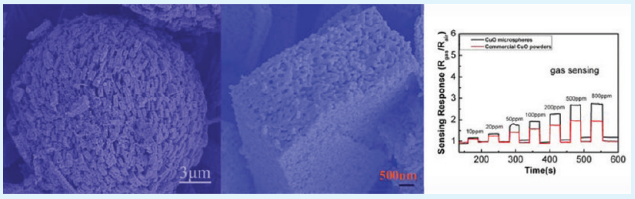

KEYWORDS: *CuO, Gas sensor, hierarchical structure, Ag-CuO, porous structure*

1. INTRODUCTION

The wide applications of gas sensors in fields such as environmental monitoring, industrial production, domestic safety, and public security have attracted many researchers worldwide for their detection of combustible and noxious gases in the air.[1−3] Transition-metal oxides are the most promising candidates for gas-sensing materials because of their low preparation cost, high stability, and high compatibility with microelectronic processing, and are being extensively studied for detecting toxic and pollutant gases like CO, NH_3, NO_2, ethanol, and acetone.[4−7] To date, many researchers have tried to find more suitable oxide materials and/or special microstructures with better gas sensing performances such as high sensitivity, fast response, and great selectivity.[8] Various nanostructured metal oxide materials, such as nanothin film,[9] nanoparticles,[10] nanotubes,[11] nanobelts,[12] and nanowires,[13] have been synthesized and investigated for sensor applications. For obtaining better performances, the sensing materials should have large surface area for sensing activation. In addition, the test gases can conveniently transport through the sensing materials. From this viewpoint, hierarchically porous structures are promising candidates because they provide a large surface-to-volume ratio and tend to form a less agglomerated configuration because of their bigger size. The analyte gases can diffuse rapidly and effectively onto the entire sensing surface via voids between building blocks, which enhance both the strength and the speed of gas response simultaneously.[1,9,14]

Among transition-metal oxides, CuO as an important *p*-type semiconductor with a narrow band gap (1.2 eV), has attracted increasing interest because of its inexpensiveness, high stability, and nontoxicity. Thus far, many efforts have been directed towards the preparation of CuO micro-/nanostructures. CuO nanoparticles,[15,16] nanorods/wires,[17−27] nanoribbons,[28−30] micro-dandelions,[31,32] nanoflowers,[33,34] hollow spheres,[35−39] nanoplates,[40,41] spindle,[42,43] nanofilms,[44] and hierarchical nanostructures[45−52] have been successfully prepared and some of them were investigated for sensing applications.[25,28,37,44,53] For example, D. Kim et al. reported the detection of hydrogen gas by porous CuO nanowires prepared with carbon nanotube template.[54] Leafletlike CuO nanosheets were found to have highly sensitive sensing to H_2S.[55] Very recently, I. Singh et al. prepared CuO nanocrystals with a sol-gel method and investigated their NH_3 sensing performances.[15] The application of CuO nanoflakes on a Cu foil through surface oxidation as high sensitive sensing of bacteria is reported by O. Akhavan et al.[41] However, up to now, few reports are about the preparation of hierarchically porous CuO structures. The hierarchically porous CuO structures are expected to show improved performances in catalysis and gas sensing because of their unique structure. Tailored preparation of the hierarchically porous CuO system is therefore a strategic subject of ongoing investigations.

In this study, we report a simple two-step method for synthesizing CuO assemblies from porous plateletlike subunits

Received: October 10, 2011
Accepted: January 18, 2012
Published: January 18, 2012

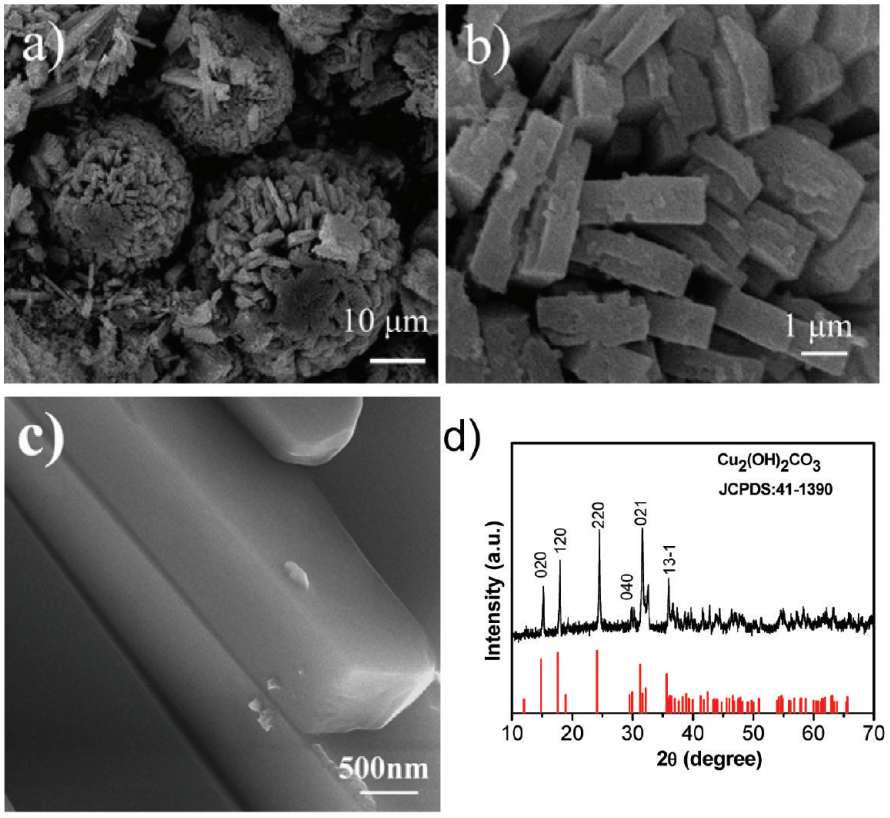

Figure 1. (a–c) SEM images of the as-synthesized $Cu_2(OH)_2CO_3$ precursor. (d) X-ray powder diffraction pattern of the as-synthesized $Cu_2(OH)_2CO_3$ precursor; the corresponding standard pattern (JCPDS: 41-1390) is also shown for comparison.

via copper basic carbonate precursor. First, the micro-spherical precursor assembled by platelet-like building blocks was prepared. The following calcination of the precursor produced hierarchical CuO architectures with openly porous feature and preservation of their premorphologies. Compared with previous reports of CuO micro-/nanostructures, our synthesis route and obtained hierarchically porous CuO microstructures have several features. (1) The source materials used in the synthesis are common inorganic salts without involving complex molecular precursors, and water as the solvent, which is cheap and green. (2) The synthesis with high concentration and high yield make it possible to get mass production. (3) The obtained hierarchical CuO microspheres are composed of many single-crystal microplatelets with open pores, which have higher stability than polycrystalline porous structure. Thus the obtained hierarchical CuO has potential application in catalysis, water treatment, lithium batteries, and sensing fields. The as-synthesized hierarchical CuO architectures were then configured as high performance chemical sensors with sensing ability toward 10 ppm level to ethanol, propanol, and acetone. The obtained hierarchical CuO assemblies show superior sensing properties to commercial CuO powder. Moreover, Ag nanoparticles were then loaded on the surface by a photochemical reduction method. The CuO architectures decorated by Ag nanoparticles display a great enhancement in gas response compared to pristine CuO architecture.

2. EXPERIMENTAL SECTION

Materials. All the chemical reagents used in our research are of analytical grade and used without further purification.

Synthesis of Hierarchically Porous CuO Microspheres. In a typical procedure, 0.01 mol of $Cu(NO_3)_2{\cdot}3H_2O$ (2.34 g), 0.03 mol of $CO(NH_2)_2$ (1.73 g) and 0.005 mol of CTAB (2 g), were orderly dissolved into 25 mL of distilled water. The mixture was vigorously stirred for 30 min and then sealed into a 30 mL of Teflon-lined stainless steel autoclave. The autoclave was heated to 120 °C and maintained for 5 h, which was allowed to cool to room temperature naturally. The as-formed precipitate, namely copper basic carbonate precursor, was separated by centrifugation, washed with distilled water and ethanol several times, and dried in vacuum at 45 °C for 10 h. The obtained precursor was further calcined in air at 450 °C for 4 h and hierarchically porous CuO microspheres were obtained.

Photochemical Deposition of Ag on Hierarchical CuO Microspheres (denoted as Ag-CuO). In a typical procedure, 0.1 g of the as-synthesized CuO was dispersed in 47 mL of deionized water with the assistance of ultrasonic irradiation. Nine milliliters of $AgNO_3$ (0.6 mmol/L) aqueous solution was then added to the suspension. The mixture was under photo-irradiation for 5 h to ensure Ag ions to be completely reduced and loaded on CuO microspheres. The obtained composites (Ag-CuO) were collected by centrifugation and washed with water and ethanol.

Characterization. The phases of the as-synthesized products were characterized using X-ray powder diffraction (XRD, Shimadzu XRD-6000) with Cu Kα radiation (λ = 1.5406 Å) at a scanning rate of 4° min^{-1}. The X-ray tubes were operated with electric current of 30 mA and voltage of 40 kV. The morphology and size of the products were examined by scanning electron microscopy (SEM, H-4800) and transmission electron microscopy (TEM, JEOL-2100). TG-DSC analysis is conducted by an integrated thermal analyzer (STA 449C) with a heating speed of 10 °C/min in air. The photochemical reaction was conducted with a DW-01 photochemical reactor, with a 500 W tungsten lamp. There is a water layer between the lamp and the reaction system to remove the infrared part of the light. The Brunauer-Emmett-Teller (BET) surface area of the CuO microsphere sample was tested using ASAP 2010 sorption analyzer. The gas sensing test is carried out on a commercial HW-30A gas sensing measurement system (HanWei Electronics Co., Ltd., Henan, China) at a relative

dx.doi.org/10.1021/am2013882 | ACS Appl. Mater. Interfaces 2012, 4, 744–751

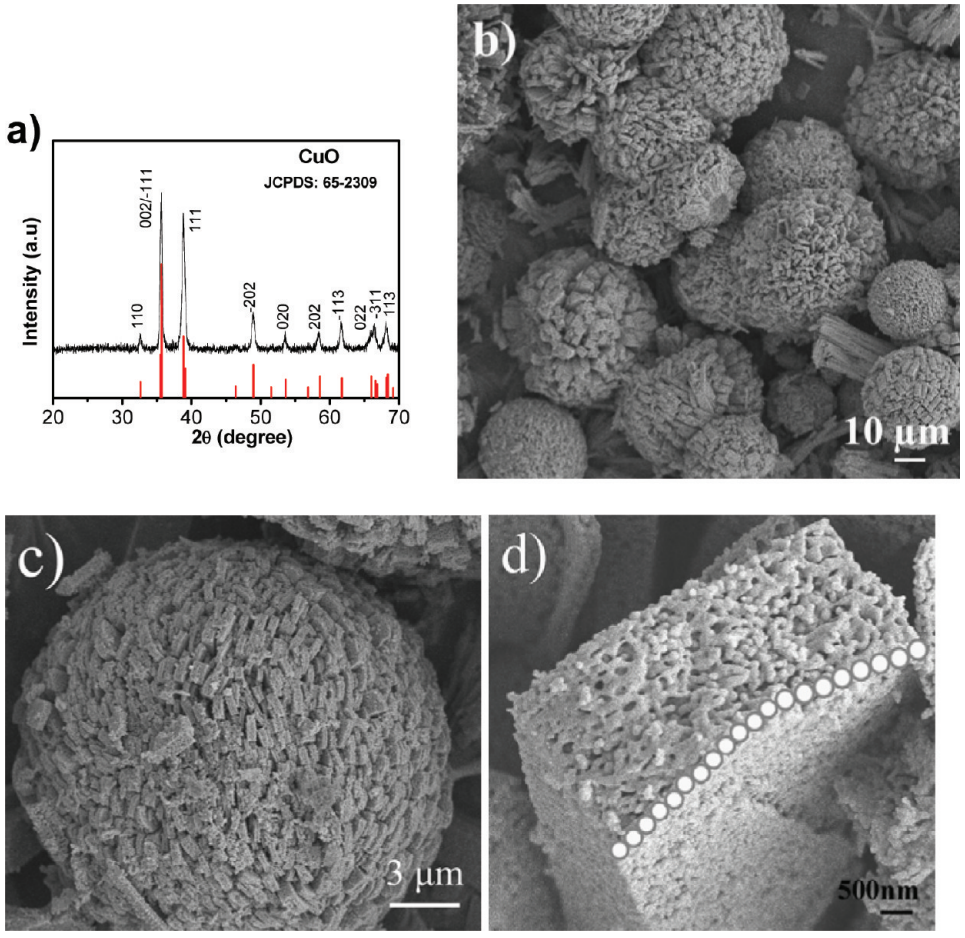

Figure 2. (a) XRD pattern of the as-synthesized CuO and the corresponding standard pattern for comparison. (b) SEM image of the obtained CuO microspheres. (c) Individual CuO microsphere clearly showing the hierarchical structure, and (d) Plateletlike CuO building block showing porous feature.

humidity of 20-30%. The fabrication and measurement of the gas sensors are the same as our reported method for In_2O_3 sensor (see Figure S1 in the Supporting Information).[56] The gas sensing response (R) is defined as the ratio of the stationary electrical resistance of the sensor in the test gas (R_{gas}) to the resistance in air (R_{air}), that is, $R = R_{gas}/R_{air}$. The measurement of resistance level and field effect characteristic is carried out on a keithley 4200 semiconductor characterization system.

3. RESULTS AND DISCUSSION

Hierarchically Porous CuO Microspheres. SEM observation was firstly performed to investigate the morphology of the as-synthesized $Cu_2(OH)_2CO_3$ precursor. As shown in Figure 1a–c, the precursor is composed of hierarchical microspheres with diameter of 24-36 μm (Figure 1a). Interestingly, the microspheres are assembled by platelet-like structures (Figure 1b). Careful observation found that the surfaces of plateletlike structures are smooth and compact without porous feature, the ends of which are not flat but with tips (Figure 1b, c). The width of the plateletlike structure is about 2.4–3.6 μm, whereas the thickness is 0.5–1 μm (Figure 1b, c).

The phase structure of the obtained precursor was determined by XRD. As shown in Figure 1d, the diffraction peaks can be indexed to monoclinic phase $Cu_2(OH)_2CO_3$ (JCPDS No. 41-1390), revealing that $Cu_2(OH)_2CO_3$ was obtained by the hydrothermal process. It is well-documented that a salt basic carbonate can be used as a precursor for the fabrication of oxide nanostructure (such as ZnO,[57] NiO,[58] Co_3O_4[59]) with preserved morphology through thermal treatment.

To determine a proper temperature for the thermal treatment, the thermal decomposition behavior of the $Cu_2(OH)_2CO_3$ precursor in air was studied using thermogravimetric-differential scanning calorimetry (TG-DSC). The obtained TG-DSC curve is shown in Figure S2 (see the Supporting Information). The only weight loss occurred at 300-400 °C (exothermic peak at 359.2 °C) can be ascribed to the decomposition of $Cu_2(OH)_2CO_3$ precursor, which releases carbon dioxide and water, and leaves the porous CuO. The curves reveal that the thermal decomposition of $Cu_2(OH)_2CO_3$ is an one-step process as reaction 1.

$$Cu_2(OH)_2CO_3 \rightarrow 2CuO + CO_2 + H_2O \quad (1)$$

From reaction 1, the estimated weight loss is 28.04%, which is in agreement with our TG experimental value 27.3%. According to this, it is concluded that the precursor can be completely decomposed above 359.2 °C to form CuO.

Thus we chose the calcination temperature of 450 °C for complete decomposition of the $Cu_2(OH)_2CO_3$ precursor into CuO. After calcination in air at 450 °C for 4 h, a black product was obtained. The XRD pattern (Figure 2a) reveals that the product is monoclinic structure CuO with lattice constants a =

dx.doi.org/10.1021/am2013882 | ACS Appl. Mater. Interfaces 2012, 4, 744–751

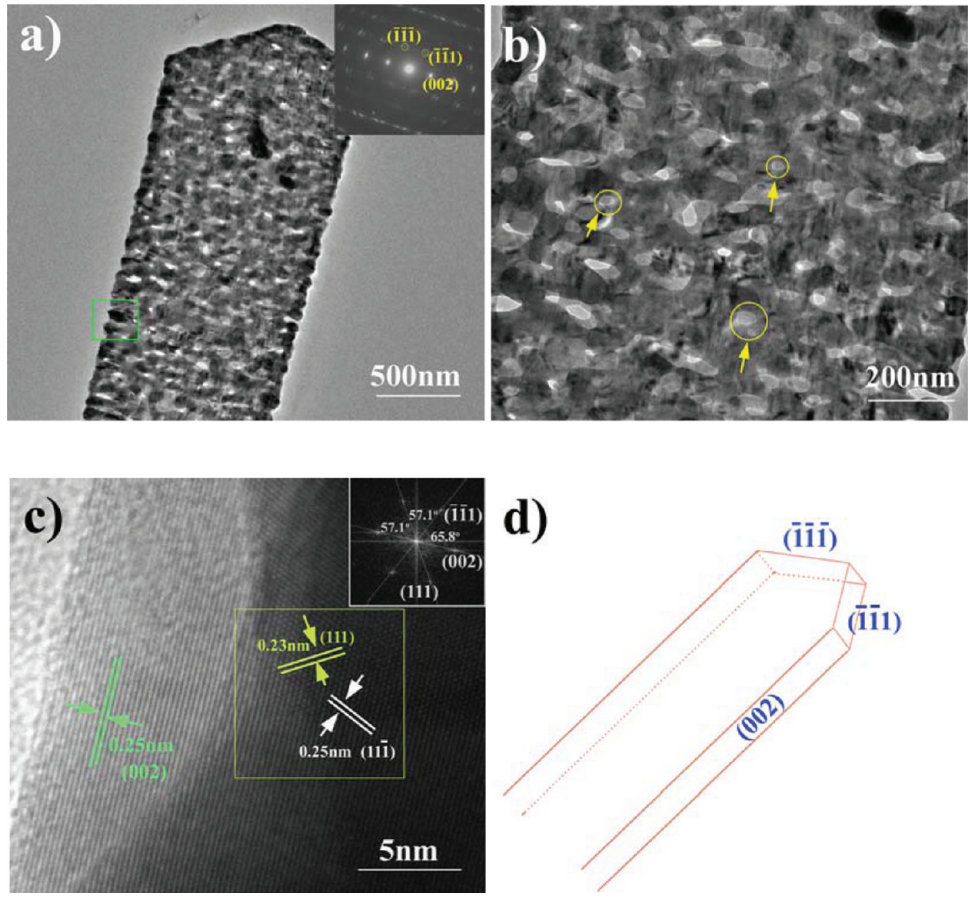

Figure 3. (a) Typical low-magnification TEM image of a platelet-like CuO, the inset is the corresponding SAED pattern. (b) TEM image with higher magnification shows the porous structural feature. (c) HRTEM image taken from the marked area in a; the inset is the corresponding fast Fourier transformation pattern demonstrating their angles of the assigned crystal surface. (d) Geometrical model of the prepared plateletlike CuO.

4.689 Å, b = 3.426 Å, and c = 5.132 Å (JCPDS No. 65-2309). The peaks at 32.6, 35.6, 38.8, 48.9, 53.5, 58.4, 61.6, 65.9, 66.4, and 68.1° correspond to the (110), (002)/(−111), (111), (−202), (020), (202), (−113), (022), (−311), and (113) lattice plane of monoclinic CuO, respectively. The diffraction peaks with high intensities indicate the higher crystallinity in nature. No characteristic peaks from the precursor is observed suggesting that the $Cu_2(OH)_2CO_3$ precursor has been completely transformed into CuO.

The morphology of the CuO product is characterized by scanning electron microscopy (SEM). Images b and c in Figure 2 display the SEM images of the corresponding CuO product after calcination. The morphology is basically preserved from the precursor. It can be seen that the product is spherical assemblies with a diameter of 13−28 μm, which consists of plenty of plateletlike building blocks. These plateletlike structural units assemble with one end growing together to form a center and another end radiating from this center forming spherical microstructure. The end of the plateletlike building blocks shows a tip structure (Figure 2d). This is similar to that of the precursor (Figure 1b). The plateletlike CuO building blocks have a thickness of 0.2−0.4 μm and a width of 0.5−1.5 μm. Not only the microsphere diameter, but also the size of the plateletlike units including their width and thickness is much smaller than that of the precursors, suggesting that the precursor has shrank during the thermal treatment process. Importantly, owing to the release of CO_2 and H_2O, the plateletlike building blocks exhibit a porous structural feature, which is in contrast to the $Cu_2(OH)_2CO_3$ precursor (Figure 1c). The high porosity of the hierarchical CuO microstructure is clearly observed from the magnified SEM images. As can be seen in Figure 2d, a large number of irregular pores are randomly distributed in the platelets. These porous structures increase the accessible surface area and facilitate the mass transport of gas in the material, which are in favor of their applications in fields such as catalyst and sensor.

The obtained CuO product is further characterized by transmission electron microscopy (TEM) and high resolution TEM (HRTEM). Figure 3a shows the TEM image of a typical platelet-like CuO building block with width of about 1.1 μm. The CuO microplatelet exhibits a tip end, which is in agreement with the SEM observation. The porous structure can also be clearly observed (Figure 3b). The pores have sizes of 20−100 nm with irregular distribution. More detailed structural information on the CuO microcrystal is provided by selected area electron diffraction (SAED) analysis and HRTEM. The corresponding SAED pattern of the CuO microcrystal is given in the inset of Figure 3a. The SAED pattern demonstrates regular dot array, indicating that the whole CuO micro-platelet is a single crystal. The diffraction dots can be assigned to the (002), (−1−1−1), (−1−11) crystal planes of monoclinic CuO. The HRTEM image recorded on the noted area in Figure 3a shows clear and continuous lattice fringes, which further establishes the single crystalline nature of the micro-platelet. In cooperation with the SAED pattern, the fringe spacings of 0.25 nm and 0.23 nm correspond to the

dx.doi.org/10.1021/am2013882 | ACS Appl. Mater. Interfaces 2012, 4, 744−751

(002) (or (11−1)) and (111) crystal planes of monoclinic phase CuO, respectively and the surface crystal planes of the CuO microcrystal are deduced. The geometrical model is shown in Figure 3d.

To further confirm the inner architecture of the hierarchically porous CuO product, we performed nitrogen adsorption and desorption measurements to estimate the texture properties. The nitrogen adsorption and desorption isotherm curve as well as the pore size distribution of hierarchically porous CuO microspheres is shown in Figure 4. The adsorption belongs to a

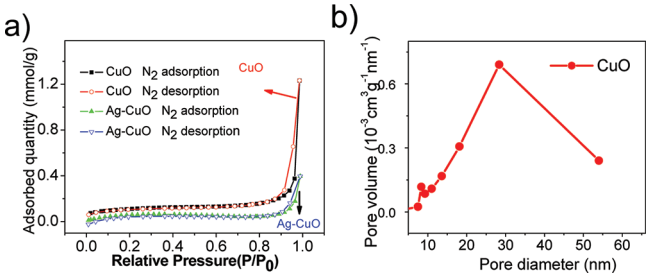

Figure 4. (a) N_2 adsorption−desorption isotherm of the obtained CuO and Ag-CuO product. (b) BJH pore size distribution curve of the obtained CuO.

multi-molecular layer type adsorption with weak interaction between N_2 and CuO. As can be seen from the adsorption curve, the N_2 adsorption quantity increases monotonically with the increasing pressure, this phenomenon usually appears in porous materials.[60] The BET specific surface area is calculated to be 12.0 m^2/g, which is much larger than that of commercial CuO powder (about 0.1 m^2/g, Figure S3, see the Supporting Information). Using the BJH method the pore diameter distribution is obtained (Figure 4b), which revealing that the main pore diameter locates at about 30 nm. This is in accordance with the microscopy observation results.

Gas Sensing. CuO is an important sensing material and has been widely used in electrical chemistry and gas sensor. We also investigated the sensing performance of the as-prepared hierarchically porous CuO microspheres. For comparison, a sensor based on commercial CuO powder was also fabricated and tested. The dc measurement of the hierarchically porous CuO sensing component is firstly conducted (Figure S4a, see the Supporting Information). The *I*−*V* plots show a linear dependence of current on applied voltage, which indicates that Ohmic contact was formed between the CuO sample and the electrodes. The Ohmic contact ensures that all upcoming sensing behaviors of the sensors originate from the CuO samples but not the contact between the sample and the electrodes. The resistance of CuO microsphere-based sensing component determined at room temperature is several hundreds of MΩ. The resistances have little change under visible-light irradiation. The characteristics of a field-effect transistor based on the sensing component are also tested and shown in Figure S4b, which shows a weak field effect. The electrical properties of these unique CuO microstructures, especially for one single microsphere or submicrometer platelet, need further investigation.

The real-time responses toward ethanol, propanol, and acetone of the two sensors are displayed in Figure 5. It can be seen that after the introducing of the reducing analyte gases, the resistances increased. The resistances of the two sensors increase abruptly on the injection of ethanol, propanol, and

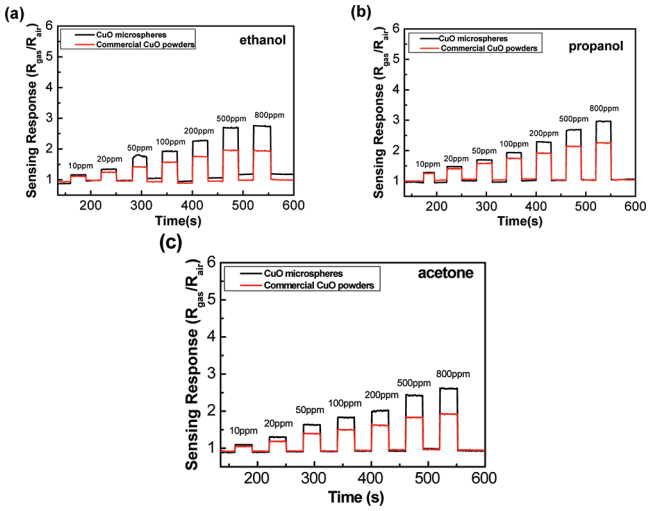

Figure 5. Real-time sensing responses toward (a) ethanol, (b) propanol, and (c) acetone of the sensors made from CuO microspheres and commercial CuO powder at operating temperature of 400 °C.

acetone, then decrease to their initial values after the test gases are released. The response magnitudes increase with increasing concentration of the test gas and that of the CuO microspheres are much higher than the commercial CuO powder. The enhanced gas response of the hierarchical nanostructures would attribute to the higher surface area for sensing reaction and the easy diffusion of tested gases endowed by the connected pores that give plenty of unblocked avenues. After many cycles between the test gas and fresh air, the resistance of the sensor could recover to its initial state, indicating that the sensor has good reversibility. The response and recovery time of CuO microsphere sensor to 200 ppm of gas (defined as the time required reaching 90% of the final equilibrium value) are only 9−17 and 4−17 s, respectively, suggesting the faster response. The response and recovery time are greatly influenced by the operation temperature. The sensor has short response and recovery times with higher operation temperature, which is related to the temperature dependent sensing reaction kinetics including the adsorption of gas on the sensing materials, and the reaction between gases and the adsorbed oxygen species. The sensing responses have little change when the sensing component is tested in dark or under visible light irradiated with a usually used incandescent lamp.

The gas sensing performance of the sensor based on the hierarchically porous CuO was also tested to 100 ppm of methanol, formaldehyde, 1,2-dichloroethane, cyclohexane, and ammonia at 400 °C. As shown in Figure 6, the sensor shows relatively lower responses to them than to ethanol, propanol, and acetone. These results indicate that the CuO microsphere gas sensor has some selectivity and may be used in exploring ethanol, propanol, and acetone gases.

It is well-known that the sensing response is greatly influenced by operating temperature owing to the temperature dependent adsorption−desorption kinetics.[61] Thus we measured the sensing performances of the CuO microspheres at different operating temperature with 100 ppm of ethanol, propanol, and acetone (Figure 7). It was found that the sensing responses decrease at higher working temperature and the optimum operating temperatures of the CuO microsphere sensor for ethanol, propanol, and acetone are 400, 300, and 300

dx.doi.org/10.1021/am2013882 | ACS Appl. Mater. Interfaces 2012, 4, 744−751

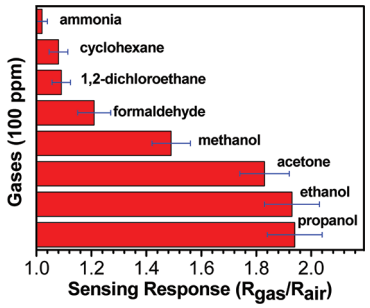

Figure 6. Gas sensing responses of the hierarchically porous CuO microspheres to 100 ppm of methanol, formaldehyde, 1,2-dichloroethane, cyclohexane, and ammonia at 400 °C.

°C, respectively. The temperature-dependence of the sensing response has been observed in many reports, which originates from several reasons. Firstly, the gas desorption and diffusion behavior through the sensing materials should be considered for this issue. Secondly, the kinetics of both the reaction of the analyte gas with surface-adsorbed oxygen and the replacement of the latter from the gas phase are two other important factors. The competition between slow kinetics at low temperatures and decreased desorption at high temperatures is believed to be responsible for this temperature-dependent sensing response, often with volcano-shaped temperature dependence of the response. When the operating temperature is too high, although the sensor has short response and recovery time because of the higher diffusion and adsorption rate of gas molecules and quick reactions between surface-adsorbed oxygen with analyte gas, the surface-adsorbed oxygen is much lower, which will decrease the response correspondingly. Sakai et al. have proposed a diffusion-controlled response model, which successfully describes these frequently observed temperature-dependent sensing responses.[62]

It has been widely accepted that the loading of metal nanoparticles such as Ag, Au, Pd, Pt on sensing materials will enhance their sensing properties because they can act as adsorption sites for analytes, or as surface catalyst. To further improve our CuO microsphere sensor, we loaded Ag nanoparticles on the surface of CuO microspheres through a photochemical reduction process (see Experimental Section). The SEM and TEM images shows that the generated Ag nanoparticles are spherical with diameter of 70−120 nm (Figure S5, see the Supporting Information). The HRTEM analysis and X-ray photoelectron energy spectrum shows that the generated nanoparticles are mainly zero-valence silver (Figures S5 and S6, see the Supporting Information. The loading amount of Ag is determined by ICP analysis, which shows that the Ag-CuO nanocomposite contains 0.4 wt % Ag. The real-time sensing responses towards ethanol, propanol, and acetone of the Ag-CuO nanocomposite sensor are also tested at 400 °C, which are similar to that of the hierarchically porous CuO microsphere sensor and are not shown here.

The corresponding responses versus the concentration of ethanol, propanol, and acetone from 10 to 800 ppm obtained from the three sensors based on the commercial CuO powder, CuO microspheres, and Ag-CuO nanocomposite are shown in Figure S7 (see the Supporting Information), from which the superiority of the Ag-CuO nanocomposite gas sensors over the two others is concluded. Although the Ag-CuO has a smaller surface area (5.0 m^2/g, Figure 4) than that of pristine hierarchical CuO microshperes, which may be caused by the deposition of Ag nanoparticles in the pores, the Ag-CuO nanocomposite sensor has much higher sensing responses for all three tested gases than the CuO microspheres and commercial CuO powder. For instance, the sensing responses of the Ag-CuO nanocomposite, CuO microspheres, and commercial CuO to 100 ppm of ethanol are 4, 1.9, and 1.6, respectively. This indicates the effective sensitive effect of Ag nanoparticles on the sensing properties. The Ag-CuO nano-

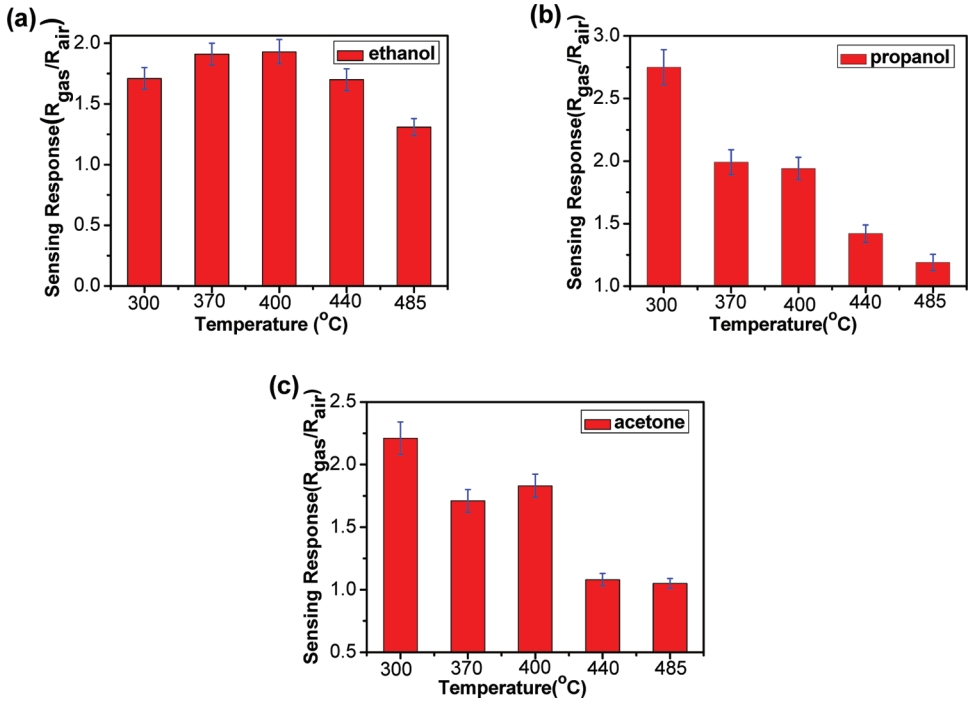

Figure 7. Sensing responses of CuO microspheres to 100 ppm of (a) ethanol, (b) propanol, and (c) acetone at different temperatures.

dx.doi.org/10.1021/am2013882 | ACS Appl. Mater. Interfaces 2012, 4, 744−751

composite sensor shows similar response and recovery times (below 20 s) to that of CuO microsphere sensor. It seems that the Ag-CuO nanocomposites are stable in our used sensing test condition. After at least seven cycles between the test gas and fresh air, the resistance of the sensor could recover to its initial state. No obvious change was observed for the resistance of the Ag-CuO sensor when keeping it under the operating temperature overnight.

This sensing enhancement phenomenon is understandable. In the air, oxygen molecules are adsorbed onto the hierarchical CuO surface forming oxygen ions (O^-, O_2^-, O^{2-}), which cause the formation of electron depletion layers on the sample surface after the chemisorption process reaches equilibrium. Because of *p*-type conductivity of CuO, the electron depletion layer will make the sensor resistance decrease. When they are exposed to the test gases, the test gases adsorb or are oxidized by the oxygen species on the CuO surface. Simultaneously, the depleted electrons are fed back to the sample, and thus the resistance increases. Then, the sensing material will restore to its original state in the air. Ag is a typical electronic-sensitization additive,[13] and easily forms a thin oxide layer (Ag_2O) on its surface in air under higher temperature, and so more electrons will be extracted from the Ag-CuO composite materials. When target gases are introduced, Ag_2O is reduced to Ag and deliver the corresponding extracted electrons. Thus in the presence of Ag nanoparticles, more electrons are extracted and then delivered, resulting in enhanced sensing response. In addition, the Ag nanoparticles would also play chemical sensitization role, promoting the gas response reaction by the dissociation of reducing gases via a spillover mechanism.[62−65]

Apart from the gas sensing application, the obtained hierarchical CuO microspheres would also have potential application as visible light driven photocatalyst for degradation of organic pollutants, since the hierarchically porous microstructures have bigger surface area and facilitate the mass transport. The following research is planned to systematically explore the photocatalytic performances of the obtained hierarchical CuO microspheres in reaction such as *p*-chloronitrobenzene degradation.

4. CONCLUSIONS

In summary, *p*-type hierarchically porous CuO microspheres have been successfully synthesized via a facile CTAB-assisted hydrothermal route followed by calcination. The prepared CuO architectures are composed of numerous plateletlike building blocks radiating from the center of the microstructure and forming a spherelike shape. The plateletlike building blocks are porous single crystals. Gas sensing tests demonstrated that the sensors based on the hierarchically porous CuO microspheres show higher responses to ethanol, propanol, and acetone in comparison with that of commercial CuO powder. The response and recovery time was below 20 s for 200 ppm of the tested gases. The loading of Ag nanoparticles on the CuO microspheres can further improve their sensing properties. The research provides a facile method for the fabrication of porous single crystal CuO architecture and highlights the potential applications of the as-prepared CuO microspheres in monitoring flammable and toxic organic gases. Such structure-induced enhancement of sensing properties could be extended to other sensing materials, and supply a chance for high-performance gas sensors.

■ ASSOCIATED CONTENT

Supporting Information

Additional figures (PDF). This material is available free of charge via the Internet at http://pubs.acs.org.

■ AUTHOR INFORMATION

Corresponding Author

*Tel: (+86)511-88791800. Fax: (+86)511-84401889. E-mail: xiaopingshen@163.com.

■ ACKNOWLEDGMENTS

The authors are grateful for financial support from the Startup Fund for Distinguished Scholars (10JDG132), the National Natural Science Foundation of China (51102117, 51072071) and China Postdoctoral Science Foundation (2011M500116).

■ REFERENCES

(1) Aronova, M. A.; Chang, K. S.; Takeuchi, I.; Jabs, H.; Westerheim, D.; Gonzalez-Martin, A.; Kim, J.; Lewis, B. *Appl. Phys. Lett.* **2003**, *83*, 1255−1257.
(2) Tiemann, M. *Chem.—Eur. J.* **2007**, *13*, 8376−8388.
(3) Tricoli, A.; Righettoni, M.; Teleki, A. *Angew. Chem., Int. Ed.* **2010**, *49*, 7632−7659.
(4) Singh, N.; Gupta, R. K.; Lee, P. S. *ACS Appl. Mater. Interfaces* **2011**, *3*, 2246−2252.
(5) Siciliano, T.; Tepore, A.; Micocci, G.; Manno, D.; Filippo, E. *Sens. Actuators, B* **2008**, *133*, 321−326.
(6) Han, X. G.; Jin, M. S.; Xie, S. F.; Kuang, Q.; Jiang, Z. Y.; Jiang, Y. Q.; Xie, Z. X.; Zheng, L. S. *Angew. Chem., Int. Ed.* **2009**, *48*, 9180−9183.
(7) Min, Y.; Gao, Q. M. *Microporous Mesoporous Mater.* **2011**, *143*, 230−235.
(8) Zhang, T; Mubeen, S.; Myung, N. V. M; Deshusses, A. *Nanotechnology* **2008**, *19*, 332001-1−14.
(9) Ishihara, T.; Higuchi, M.; Takagi, T.; Ito, M.; Nishiguchi, H.; Takita, Y. *J. Mater. Chem.* **1998**, *8*, 2037−2042.
(10) Zhang, G.; Liu, M. *Sens. Actuators, B* **2000**, *69*, 144−152.
(11) Sayago, I.; Santos, H.; Horrillo, M. C.; Aleixandre, M.; Fernández, M. J.; Terrado, E.; Tacchini, I.; Aroz, R.; Maser, W. K.; Benito, A. M.; Martínez, M. T.; Gutiérrez, J.; Munoz, E. *Talanta* **2008**, *77*, 758−764.
(12) Comini, E.; Faglia, G.; Sberveglieri, G.; Zheng, W. P.; Wang, Z. L. *Appl. Phys. Lett.* **2002**, *81*, 1869−1871.
(13) Hwang, I.; Choi, J. K.; Woo, H. S.; Kim, S. J.; Jung, S. Y.; Seong, T. Y.; Kim, I. D.; Lee, J. H. *ACS Appl. Mater. Interfaces* **2011**, *3*, 3140−3145.
(14) Zeng, Y.; Zhang, T.; Fan, H. T.; Fu, W. Y.; Lu, G. Y.; Sui, Y. M.; Yang, H. B. *J. Phys. Chem.C* **2009**, *113*, 19000−19004.
(15) Bedi, R. K.; Singh, I. *ACS Appl. Mater. Interfaces* **2010**, *2*, 1361−1368.
(16) Babu, S. G.; Karvembu, R. *Ind. Eng. Chem. Res.* **2011**, *50*, 9594−9600.
(17) Kim, Y. S.; Hwang, I. S.; Kim, S. J.; Lee, C. Y.; Lee, J. H. *Sens. Actuators, B* **2008**, *135*, 298−303.
(18) Wang, C.; Fu, X. Q.; Xue, X. Y.; Wang, Y. G.; Hwang, T. *Nanotechnology* **2007**, *18*, 145506−1-5.
(19) Liao, L.; Zhang, Z.; Yan, B.; Zheng, Z.; Bao, Q. L.; Wu, T.; Li, C. M.; Shen, Z. X.; Zhang, J. X.; Gong, H.; Li, J. C.; Yu, T. *Nanotechnology* **2009**, *20*, 085203−1-6.
(20) Jiang, X. C.; Herricks, T.; Xia, Y. N. *Nano Lett.* **2002**, *2*, 1333−1338.
(21) Shrestha, K. M.; Sorensen, C. M.; Klabunde, K. J. *J. Phys. Chem. C* **2010**, *114*, 14368−14376.
(22) Wen, X.; Xie, Y.; Choi, C. L.; Wan, K. C.; Li, X. Y.; Yang, S. *Langmuir* **2005**, *21*, 4729−4737.
(23) Li, J. Y.; Xiong, S. L.; Xi, B. J.; Li, X. G.; Qian, Y. T. *Cryst. Growth Des.* **2009**, *9*, 4108−4115.

(24) Wang, F.; Tao, W. Z.; Zhao, M. S.; Xu, M. W.; Yang, S. C.; Sun, Z. B.; Wang, L. Q.; Song, X. P. *J. Alloys Compd.* **2011**, *509*, 9798−9803.
(25) Yang, C.; Su, X. T.; Xiao, F.; Jian, J. K.; Wang, J. D. *Sens. Actuators, B* **2011**, *158*, 299−303.
(26) Wang, Y.; Shen, R. Q.; Jin, X. Y.; Zhu, P.; Ye, Y. H.; Hu, Y. *App. Surf. Sci.* **2011**, *258*, 201−206.
(27) Zhang, X. J.; Shi, W. H.; Zhu, J. X.; Kharistal, D. J.; Zhao, W. Y.; Lalia, B. S.; Hng, H. H.; Yan, Q. Y. *ACS Nano* **2011**, *5*, 2013−2019.
(28) Gou, X.; Wang, G.; Yang, J.; Park, J.; Wexler, D. *J. Mater. Chem.* **2008**, *18*, 965−969.
(29) Wang, X. Q.; Xi, G. C.; Xiong, S. L.; Liu, Y. K.; Xi, B. J.; Yu, W. C.; Qian, Y. T. *Cryst. Growth Des.* **2007**, *7*, 930−934.
(30) Chang, Y.; Zeng, H. C. *Cryst. Growth Des.* **2004**, *4*, 397−402.
(31) Liu, B.; Zeng, H. C. *J. Am. Chem. Soc.* **2004**, *126*, 8124−8125.
(32) Manna, S.; Das, K.; De, S. K. *ACS Appl. Mater. Interfaces* **2010**, *2*, 1536−1542.
(33) Song, M. J.; Hwang, S. W.; Whang, D. *Talanta* **2010**, *80*, 1648−1652.
(34) Gao, D. Q.; Yang, G. J.; Li, J. Y.; Zhang, J.; Zhang, J. L.; Xue, D. S. *J. Phys. Chem. C* **2010**, *114*, 18347−18351.
(35) Titirici, M. M.; Antonietti, M.; Thomas, A. *Chem. Mater.* **2006**, *18*, 3808−3812.
(36) Zhang, Z. K.; Guo, D. Z.; Zhang, G. M. *J. Colloid Interface Sci.* **2011**, *357*, 95−100.
(37) Zhang, Y.; He, X. L.; Li, J. P.; Zhang, H. G.; Gao, X. G. *Sens. Actuators, B* **2007**, *128*, 293−298.
(38) Wang, S. L.; Xu, H.; Qian, L. Q.; Jia, X.; Wang, J. W.; Liu, Y. Y.; Tang, W. H. *J. Solid State Chem.* **2009**, *182*, 1088−1093.
(39) Kong, M.; Zhang, W. X.; Yang, Z. H.; Weng, S. Y.; Chen, Z. X. *Appl. Surf. Sci.* **2011**, *258*, 1317−1321.
(40) Zhou, K. B.; Wang, R. P.; Xu, B. Q.; Li, Y. D. *Nanotechnology* **2006**, *17*, 3939−3943.
(41) Akhavan, O.; Ghaderi, E. *J. Mater. Chem.* **2011**, *21*, 12935−12940.
(42) Li, J. P.; Sun, F. Q.; Gu, K. Y.; Wu, T. X.; Zhai, W.; Li, W. S.; Huang, S. F. *Appl. Catal. A* **2011**, *406*, 51−58.
(43) Liu, X.; Zhang, J.; Kang, Y.; Wu, S.; Wang, S. *CrystEngComm* **2012**, *14*, 620−625.
(44) Barreca, D.; Comini, E.; Gasparotto, A.; Maccato, C.; Sada, C.; Sberveglieri, G.; Tondello, E. *Sens. Actuators, B* **2009**, *141*, 270−275.
(45) Gao, S. Y.; Yang, S. X.; Shu, J.; Zhang, S. X.; Li, Z. D.; Jiang, K. *J. Phys. Chem. C* **2008**, *112*, 19324−19328.
(46) Zhang, Y. J.; Or, S. W.; Wang, X. L.; Cui, T. Y.; Cui, W. B.; Zhang, Y.; Zhang, Z. D. *Eur. J. Inorg. Chem.* **2009**, *48*, 168−173.
(47) Wang, Y. Q.; Meng, D. W.; Liu, X. Q.; Li, F. *Cryst. Res. Technol.* **2009**, *44*, 1277−1283.
(48) Sun, J. H.; Jia, Y. Z.; Jing, Y.; Yao, Y.; Ma, J.; Gao, F.; Xia, C. L. *J. Nanosci. Nanotechnol.* **2009**, *9*, 5903−5909.
(49) Zhu, L. J.; Chen, Y. T.; Zheng, Y. T.; Li, N. X.; Zhao, J. D.; Sun, Y. G. *Mater. Lett.* **2010**, *64*, 976−979.
(50) Akhavan, O.; Azimirad, R.; Safa, S.; Hasani, E. *J. Mater. Chem.* **2011**, *21*, 9634−9640.
(51) Xiang, J. Y.; Tu, J. P.; Qiao, Y. Q.; Wang, X. L.; Zhong, J.; Zhang, D.; Gu, C. D. *J. Phys. Chem. C* **2011**, *115*, 2505−2513.
(52) Deng, C. H.; Hu, H. M.; Zhu, W. L.; Han, C. L.; Shao, G. Q. *Mater. Lett.* **2011**, *65*, 575−578.
(53) Aslani, A.; Oroojpour, V. *Phys. B* **2011**, *406*, 144−149.
(54) Hoa, N. Y.; Quy, N. Y. V.; Jung, H.; Kim, D. *Sens. Actuators, B* **2010**, *146*, 266−272.
(55) Zhang, F.; Zhu, A. W.; Luo, Y. P.; Tian, Y.; Yang, J. H.; Qin, Y. *J. Phys. Chem. C* **2010**, *114*, 19214−19219.
(56) Guo, L. J.; Shen, X. P.; Zhu, G. X.; Chen, K. M. *Sens. Actuators, B* **2011**, *155*, 752−758.
(57) Wang, X. B.; Cai, W. P.; Lin, Y. X.; Wang, G. Z. *J. Mater. Chem.* **2010**, *20*, 8582−8590.
(58) Ding, S.; Zhu, T.; Chen, J. S.; Wang, Z.; Yuan, C.; Lou, X. W. *J. Mater. Chem.* **2011**, *21*, 6602−6606.
(59) Xie, X. W.; Li, Y.; Liu, Z. Q.; Haruta, M.; Shen, W. J. *Nature* **2009**, *458*, 746−749.
(60) Asuha, S.; Suyala, B.; Zhao, S. *Mater. Chem. Phys.* **2011**, *129*, 483−487.
(61) Pitois, A.; Pilenga, A.; Pfrang, A.; Tsotridis, G. *Int. J. Hydrogen Energy* **2011**, *36*, 4375−4385.
(62) Sakai, G.; Matsunaga, N.; Shimanoe, K.; Yamazoe, N. *Sens. Actuators, B* **2001**, *80*, 125−131.
(63) Yamazoe, N. *Sens. Actuators, B* **1991**, *5*, 7−19.
(64) Shukla, S.; Seal, S.; Ludwig, L.; Parish, C. *Sens. Actuators, B* **2004**, *97*, 256−265.
(65) Joshi, R. K.; Kruis, F. E. *Appl. Phys. Lett.* **2007**, *89*, 153116−1-3.